Examining the spectroscopic features and quantum chemical computations of a Quinoline derivative: Experimental and theoretical insights into the photophysical characteristics

Kalpana Sharma[a], Raveendra Melavanki[a*], V T Muttannavar[b], J Thipperudrappa[c], N R Patil[d] & Raviraj Kusanur[e]

[a]Department of Physics, M S Ramaiah Institute of Technology, Bangaluru 560 054, India
[b]Department of Physics, J S S Science RSH PU College, Vidyagiri Dharwad 580 003, India
[c]Post Graduation Studies in Physics, Vijayanagar Sri Krishna Devaraya University,VSKU, Bellary 583 104, India
[d]Department of Physics, B V B College of Engineering & Technology, Hubli 580 031, India
[e]Department of Chemistry, R V College of Engineering, Bangalore 560 059, India

The solvatochromic studies in a Quinoline derivative molecule namely Quinolin-8-ol (QO) have been carried out at ambient temperature using absorption and fluorescence spectroscopy. The QO molecule shows the bathochromic shift with increase in solvent polarity demonstrating $\pi \rightarrow \pi^*$ transition. The solvatochromic data coupled with quantum mechanical calculations has been used to estimate change in dipole moment of the molecule after excitation. It has been found that excited state dipole moment is greater than the corresponding ground state dipole moment. Further, it is observed that excited and ground state dipole moments are parallel. The chemical reactivity and kinetic stability of QO molecule are investigated using Frontier molecular orbital (FMO) analysis. Natural bond orbital (NBO) analysis shows proton transfer within the selected donor-acceptor depicting large energy of stabilization for QO molecule. The calculated Fukui functions infer the local softness and local eletrophilicity index of QO molecule. The theoretically simulated UV-Vis absorption spectrum of QO molecule matches well with the experimental spectrum.

Keywords: Solvatochromic studies, Ground and excited state dipole moments, FMO, MEP, NBO, Fukui functions, Ultraviolet-visible spectral analysis

1 Introduction

Quinoline derivatives[1-3] belong to a family of dyes which have significant role in emerging areas of science and technology. These molecules are widespread in a variety of pharmacologically active synthetic and natural compounds. Also these molecules have shown antiseptic, antipyretic, antiperiodic properties and are used as antimalarials. These properties are made these molecules suitable for the development of new drugs. Apart from wide range of biological and pharmacological activities, these molecules have industrial applications such including corrosion inhibitors, preservatives, alkaloids, rubber chemicals, flavouring agents and solvents for resins and terpenes. Further, these molecules have remarkable applications in dye industry due to their strong fluorescence in UV-visible region[4-8]. The excellent biological activities of these molecules coupled with their fluorescence could be used for the development of bio-analytical systems/devices including bio sensors. The development of these systems/devices needs thorough understanding of photophysical behaviour in different environments. This is the motivation behind taking up this research work. In this paper we have presented solvatochromic studies and measurement of excited state dipole moments. Also the DFT/B3LYP method is used to explicate optimized molecular structure, Natural bond orbital (NBO), Frontier molecular orbitals (FMOs), total electron density mapped with the molecular electrostatic potential (MEP) surface, Fukui functions and UV-visible studies using Gaussian 09 program.

2 Theory

2.1. Experimental determination of ground and excited state dipole moments

The excited state dipole moment of the compound is estimated from three independent equations which are as follows:

Lippert's equation,

$$(\overline{\nu}_a - \overline{\nu}_f) = m_1 F_1(\varepsilon, n)^{+ \text{constant}} \qquad \dots (1)$$

*Corresponding authors (E-mail: melavanki73@gmail.com)

Bakhshiev's equation[11]

$$(\overline{V}_a - \overline{V}_f) = m_2 F_2(\varepsilon, n) + \text{constant} \qquad \dots (2)$$

Kawski-Chamma-Viallet'sequation

$$\frac{(\overline{V}_a + \overline{V}_f)}{2} = m_3 F_3(\varepsilon, n) + \text{constant} \qquad \dots (3)$$

$F_1(\varepsilon,$ n) [Lippert's polarity equation], $F_2(\varepsilon,$ n) [Bakhshiev's polarity equation], $F_3(\varepsilon,$ n) and [Kawski-Chamma-Viallet's polarity equation] are expressed as:

$$F_1(\varepsilon,n) = \left[\frac{\varepsilon - 1}{2\varepsilon + 1} - \frac{n^2 - 1}{2n^2 + 1} \right] \qquad \dots (4)$$

$$F_2(\varepsilon,n) = \left[\frac{\varepsilon - 1}{\varepsilon + 2} - \frac{n^2 - 1}{n^2 + 2} \right] \frac{(2n^2 + 1)}{(n^2 + 2)} \qquad \dots (5)$$

$$F_3(\varepsilon,n) = \frac{2n^2 + 1}{2(n^2 + 2)} \left[\frac{\varepsilon - 1}{\varepsilon + 2} - \frac{n^2 - 1}{n^2 + 2} \right] + \frac{3(n^4 - 1)}{2(n^2 + 2)^2} \qquad \dots (6)$$

Where $\overline{v}_a$ and $\overline{v}_f$ are absorption and fluorescence maxima wavenumbers in cm^{-1} respectively. The ε and n denote the dielectric constant and refractive index of solvents respectively in above equations. From Eqs (1)-(3) it is clear that plot of $(\overline{V}_a - \overline{V}_f)$ versus $F_1(\varepsilon,$ n), $(\overline{V}_a - \overline{V}_f)$ versus $F_2(\varepsilon,$ n) and ½ $(\overline{V}_a + \overline{V}_f)$ versus $F_3(\varepsilon,$ n) should be linear with slopes m_1, m_2 and m_3 respectively and are given as:

$$m_1 = \frac{2(\mu_e - \mu_g)^2}{hca^3} \qquad \dots (7)$$

$$m_2 = \frac{2(\mu_e - \mu_g)^2}{hca^3} \qquad \dots (8)$$

$$m_3 = \frac{2(\mu^2_e - \mu^2_g)}{hca^3} \qquad \dots (9)$$

where, ground and excited state dipole moments are symbolized by μ_g and μ_e of the dye molecules. The symbols ′h′ and ′c′ have their usual meanings and 'a' is Onsager cavity radius of the solute. If the ground state and excited state dipole moments are parallel, following expressions are obtained on the basis of Eqs (8) and (9).

$$\mu_g = \frac{m_3 - m_2}{2} \left[\frac{hca^3}{2m_2} \right]^{1/2} \qquad \dots (10)$$

$$\mu_e = \frac{m_3 + m_2}{2} \left[\frac{hca^3}{2m_2} \right]^{1/2} \qquad \dots (11)$$

and

$$\mu_e = \left[\frac{m_2 + m_3}{m_3 - m_2} \right] \mu_g \qquad \text{for } m_3 > m_2 \qquad \dots (12)$$

If dipole moments μ_e and μ_g are not parallel to each other but form an angle ϕ, then ϕ can be calculated using Eq.

$$\cos \phi = \frac{1}{2\mu_g \mu_e} \left[(\mu_g^2 + \mu_e^2) - \frac{m_3}{m_2} (\mu_e^2 - \mu_g^2) \right] \qquad \dots (13)$$

2.2. Molecular-microscopic solvent polarity parameter (E_T^N)

To study solvatochromic shift of dipolar molecule, an empirical polarity parameter E_T^N given by Reichardt gives dependence of polarization or effect of hydrogen bonding on spectral characteristics. Microscopic solvent polarity E_T^N, which involves dielectric constant (ε) and refractive index (n) can correlate spectral shift in a better way as compared to traditionally used bulk solvent polarity function. This polarity scale takes into account the intermolecular solute/solvent hydrogen bond donor/acceptor interactions along with solvent polarity and the difficulty comprising the estimation of Onsager cavity radius 'a' has been reduced in this method. The change in dipole moment of QO molecule is also estimated using the dependence of spectral band shift with an empirical polarity parameter E_T^N given by Reichardt and developed by Ravi *et al*. The dependence of spectral band shift with an empirical polarity parameter E_T^N is given in equation[14]

$$\overline{V}_a - \overline{V}_f = 11307.6 \left[\left(\frac{\Delta\mu}{\Delta\mu_b} \right)^2 \left(\frac{a_B}{a} \right)^3 \right] + E_T^N + \text{constant} \qquad \dots (14)$$

where $\Delta\mu_b = 9D$ and $a_B = 6.2A^0$ are the change in dipole moment on excitation and Onsager cavity radius of betaine dye molecule respectively. Here

$\Delta\mu$ and $'a'$ are the corresponding quantities for the molecule of interest. By using the slope obtained from the plot of Stokes shift $(\overline{v}_a - \overline{v}_f)$ versus microscopic solvent polarity (E_T^N) using Eq.(14), change in dipole moment can be calculated. The microscopic solvent polarity parameter (E_N^T) value of solvents are taken from literature.

2.3 Quantum chemical computational studies

Quantum chemical computations are carried out by using DFT/B3LYP method with 6-311++G (d, p) basis set via Gaussian 09W. The ground state dipole moment was calculated in gas phase. The geometry of QO molecule was fully optimized using Gauss view database by gradient geometry optimization. Electronic properties including frontier molecular orbital energies (E_{HOMO} and E_{LUMO}), MEP, surface contour map, Mulliken charges, Fukui function calculations and UV-visible spectra were examined by DFT with 6-311++G (d, p) basis level in the gas phase. NBO version 5.0 is used to study NBO computation for the investigated molecule.

3   Materials and Methods

3.1   Materials

The Quinolin-8-ol (QO) molecule was synthesized in our laboratory using standard methods[1-3]. The molecular structure of QO is shown in Fig. 1. The solvents used in the present study namely butanol (BL), dimethyl formamide (DMF), dimethyl sulphoxide (DMSO), acetonitrile (AN), methanol (ML), ethanol (EL), propanol (PL), toluene (TL) and 1-4 dioxane (DX)were obtained from S-D-Fine Chemicals Ltd., India and they were of spectroscopic grade.

3.2 Measurement of absorption and fluorescence spectra

The absorption spectra were recorded using Labomed UV 3600 spectrophotometer over a wavelength range 200–700 nm and fluorescence spectra were recorded using Hitachi F-2700
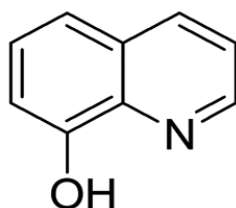
Spectroflourimeter with standard quartz cuvette at room temperature. The uncertainty in the measured wavelength of absorption and fluorescence maxima is ±1 nm. Every time freshly prepared homogenous solution was used for recording both absorption and fluorescence spectra by keeping concentrations 1×10^{-4}M in all solvents.

4   Results and Discussion

4.1   Analysis of Photophysical behavior: An experimental ground and excited state dipole moments

4.1.1   Solvent effect on absorption and fluorescence emission spectra

The typical absorption and fluorescence spectra of QO molecule in 1,4 - dioxane are depicted in Figs 2 and 3 respectively. The absorption maxima and emission maxima in different solvents are listed in Table 1. The absorption maximum has shown blue shift with change in solvent from non-polar toluene to polar alcohols.
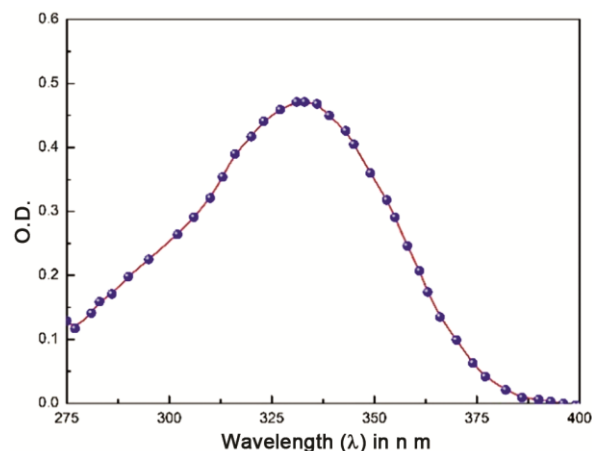

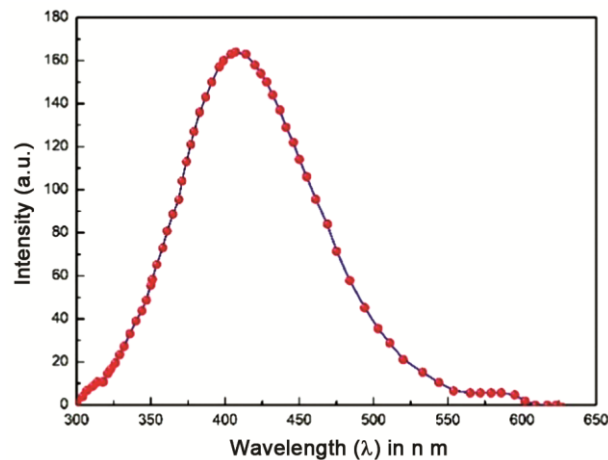Fig. 2 – Typical absorption spectrum of QO in 1,4-Dioxane

Fig. 1 – Molecular Structures of QO

Fig. 3 – Typical emission spectra for QO in 1,4-Dioxane

Table 1 – Photo physical parameters of QO in different solvents.

Solvents	$\lambda_a(nm)$	$\lambda_e(nm)$	$\bar{v}_a(cm^{-1})$	$\bar{v}_f(cm^{-1})$	$(\bar{v}_a - \bar{v}_f)$ (cm^{-1})	$(\bar{v}_a + \bar{v}_f)/2$ (cm^{-1})
BL	304.86	406.5	32801.94	24600.25	8201.70	28701.09
TL	328	401	30487.8	24937.66	5550.15	27712.73
ML	303.14	398	32988.06	25125.63	7862.43	29056.84
EL	308	407	32467.53	24570.02	7897.51	28518.78
AN	305.3	398.5	32754.67	25094.1	7660.56	28924.39
DX	330.71	401.5	30237.97	24906.6	5331.37	27572.29
PL	298.86	406	33460.48	24630.54	8829.94	29045.51
DMF	320	341.5	31250	29282.58	1967.42	30266.29
DMSO	300	355	33333.33	28169.01	5164.32	30751.17

The excitation maximum coincides with the longest wavelength absorption band and this longest wavelength absorption band has been assigned as the intermolecular charge transfer transition. The absorption and emission maxima shifts to the longer wavelengths with increase in solvent polarity. The absorption and emission maxima, Stokes shift and arithmetic mean of Stokes shift values for QO molecule in different solvents are given in Tables 1 and 2. The emission spectra show a maximum around 390-495nm with a shift of the maximum depending on the solvent used. It is observed that absorption band shift is less with change in solvent polarity, indicating ground state energy distribution is not affected to a greater extent as the ground state is less polar than in the excited state.

The large magnitude of Stokes shift shows the different geometry of excited state geometry as compare to the ground state. It has been observed that with increase in solvent polarity, Stokes shift values also increases which clearly indicates the increment in the dipole moment on excitation. Spectra can be detected using the solvatochromic data. It can be observed from the Tables 1 and 2 that, π→π* transition is confirmed by bathochromic shift of fluorescence emission peak with the increase in the polarity of the solvent. The noticeable difference of charge distribution of excited state as compared to ground state may attribute to shift of the fluorescence wavelengths towards longer wavelengths and leads to stronger interaction in the excited state with polar solvents.

4.1.2 Experimental Excited-state dipole moments

Tables 1 and 2 summarize the band shift data along with the solvent polarity function values F_1(ε,n), F_2 (ε,n), and F_3 (ε,n) of various solvents for respective molecules. The linear graphs of $\bar{v}_a - \bar{v}_f$

Table 2 – Dielectric constant (ε), refractive index (n), solvent polarity functions, microscopic solvent polarity parameter (E_T^N) for QO.

Solvents	ε	n	$F_1(\varepsilon,n)$	$F_2(\varepsilon,n)$	$F_3(\varepsilon,n)$	E_N^T
BL	17.5	1.39	0.2667	0.7535	0.6419	0.586
TL	2.408	1.49	0.0178	0.0391	0.3504	0.099
ML	32.51	1.32	0.3117	0.8565	0.6463	0.762
EL	24.35	1.35	0.2927	0.8154	0.6460	0.654
AN	35.87	1.34	0.3061	0.8602	0.6617	0.460
DX	2.219	1.41	0.0256	0.0514	0.3041	0.164
PL	20.68	1.38	0.2765	0.7834	0.6502	0.617
DMF	38.5	1.42	0.2788	0.8431	0.7067	0.404
DMSO	47.24	1.47	0.2661	0.8442	0.7400	0.444

versus F_1(ε,n), $\bar{v}_a - \bar{v}_f$ versus F_2(ε,n) and $\frac{1}{2}(\bar{v}_a + \bar{v}_f)$ versus F_3(ε,n) are given in Figs 4-6. The correlation coefficients and slopes m_1, m_2 and m_3 of the fitted lines are given in Table 3. The excited state dipole moments of compounds are estimated using Eq. (1-3) from the values of slopes for Lippert's, Bakshiev and Kawski-Chamma-Viallet's listed in Table 5 and Onsager cavity radius 'a' of the solute compound values calculated from the molecular volume as shown in Table 4. For all the cases, we have found a good value of correlation coefficient. Several researchers reported negative value of m_3, but we obtained positive value of m_3 for this used compound which is in agreement with results of many reports[9-12].The theoretical and experimental values of ground state (μ_g) and excited state (μ_e) dipole moments predicted using Eq. are shown in Table 4.

In the studied molecule, μ_e is greater than μ_g, which indicates that μ_g and μ_e are parallel. The angle between μ_g and μ_e calculated according to Eq.[13-15] and the value is found to be 0^0 for this compound. The values $\Delta\mu$ and the ratio (μ_e/μ_g) for compound is given in Table 4. The enhancement in the dipole moment of compound on excitation can be explained in terms of nature of emitting state or intra molecular charge

transfer. Moreover, a huge change in dipole moment on excitation suggests twisted intra molecular charge transfer (TICT) in excited state. Thus the compound has large change in dipole moment and hence become more polar due to presence of large TICT and with increment in linearity on excitation. Table 6 shows difference in the theoretical and estimated values of μ_e for studied compound. Also, value of dipole moment
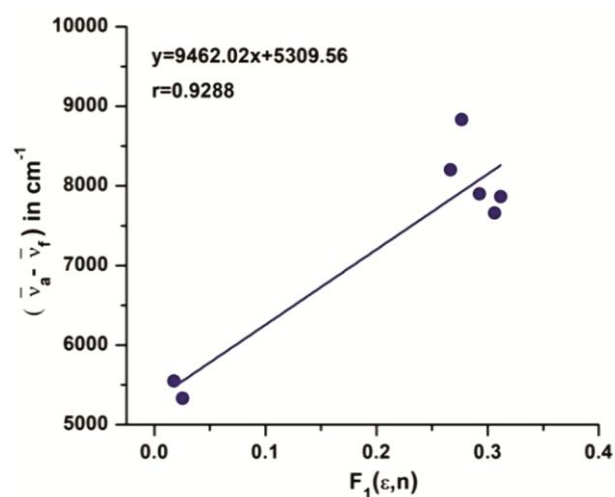

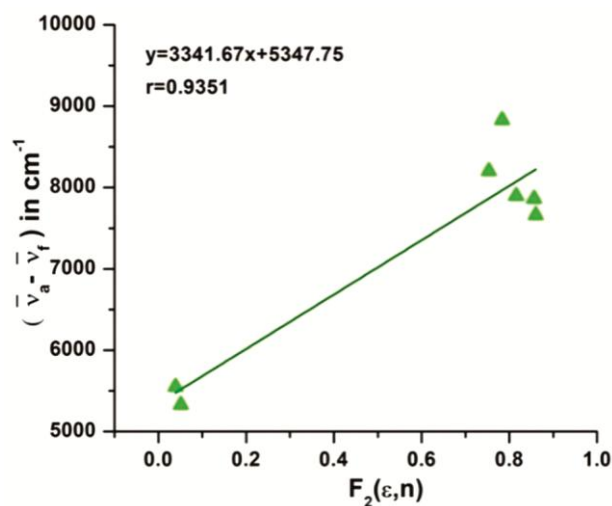Fig. 4 – The variation of Stoke's shift with F_1 (ε, n) using Lippert equation for QO

Fig. 5 – The variation of Stoke's shift with F_2 (ε, n) using Bakshiev's equation for QO

for excited state predicted from Lippert*'s* method is large as compared to other methods.

4.1.3 Molecular-Microscopic Solvent Polarity Parameter (E_T^N)

The plot of Stoke's shift as a function of E_T^N in all the solvents for this compound are shown in Fig. 7. The linear dependence of Stoke's shift on E_T^N specifies the general type of solute-solvent interaction to be present in which the Stoke's shift depends on the dielectric constant and refractive index of the solvents. Using microscopic solvent polarity parameter (E_T^N), the excited state dipole moment represented as $\mu_e{}^g$ in Table 4 is also calculated according to Eqn[16-33].

The values of excited state dipole moment μ_e using solvent polarity parameter E_T^N is less for QO as compared to Lippert's, Bakshiev and Kawski-Chamma-Viallet's equation. As the Lippert's, Bakshiev and Kawski-Chamma-Viallet's equations do not consider specific solute solvent interactions such as hydrogen bonding effect, complex formation and also ignore molecular aspects of solvation, whereas these aspects are incorporated in the method based on E_T^N. This indicates ICT (intermolecular charge transfer) observed in Quinoline compound QO.
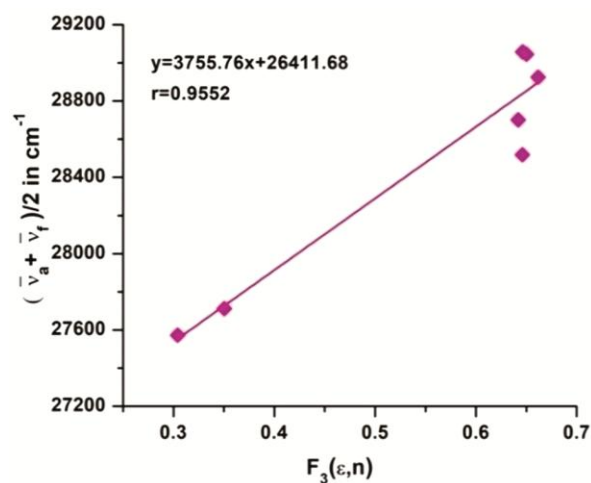

Fig. 6 – The variation of arithmetic means of Stoke's shift with F_3 (ε, n) using Kawski- Chamma-Viallet's equation for QO

Table 3 – Statistical treatment of the correlations of solvents spectral shifts of QO					
Compounds	Method	Slope	Intercept	Correlation factor 'r'	Number of data (N)
QO	Lippert Correlation	9462.02	5309.56	0.92	7
	Bakhshiev's Correlation	3341.67	5347.75	0.93	7
	Kawaski-Chamma-Viallet Correlation	3755.77	264111.68	0.95	7
	Reichards Correlation	4802.80	5040.38	0.90	7

Table 4 – Ground state and excited state dipole moments of QO.

Compound	Radius 'a'(Å)	μ_g^a (D)	μ_g^b (D)	μ_e^c (D)	μ_e^d (D)	μ_e^e (D)	μ_e^f (D)	μ_e^g (D)	μ_e^h (D)	$\Delta\mu^i$	$\Delta\mu^j$	$\left(\dfrac{\mu_e}{\mu_g}\right)^k$	Φ^l
QO	3.157	2.814	0.200	3.872	3.433	5.639	3.433	3.533	2.331	3.232	2.131	17.139	0°

Debye (D) =3.33564x10-30 cm=10^{-18}esu cm.
a The ground states dipole moments calculated using Gaussian software.
b The ground states dipole moments calculated using Eq.(7)
c The excited states dipole moments calculated using Gaussian software.
d The excited states dipole moments calculated using Eq.(8)
e The experimental excited states dipole moments calculated from Lippert's equation.
f The experimental excited states dipole moments calculated from Bakshiev's equation.
g The experimental excited states dipole moments calculated from Kawaski-Chamma-Viallet equation.
h The excited states dipole moments calculated from E_N^T equation.
i The change in dipole moments for μ_e and μ_g.
j The change in dipole moments calculated from Eq.(16).
k The ratio of excited state and ground state dipole moment.
l The angle between ground state and excited state dipole moments calculated using Eq.(13)

Table 5 – Calculated FMOs and related molecular properties values of the QO.

Molecular properties	Energy (in eV) for QO
HOMO	-6.118
LUMO	-1.899
E_{HOMO}-E_{LUMO}	4.219
Ionization potential (IP)	6.118
Electron affinity(EA)	1.899
Electronegativity(χ)	4.008
Hardness(η)	2.110
Softness(S)	0.474
Chemical potential(μ)	-4.008
Electrophilicity index(ω)	3.808

Table 6 – Calculated Mulliken atomic charge distribution of QO.

Atoms	Mulliken atomic charge distribution		
	Anion q(N-1)	Neutral q(N)	Cation q(N+1)
C1	-0.1832	-0.1606	-0.1768
C2	-0.1072	-0.0257	0.1347
C3	2.0355	2.1327	2.2094
C4	-1.7871	-1.9084	-1.9939
C5	-0.7877	-0.8144	-0.7820
C6	0.1416	0.1643	0.2007
H7	0.1010	0.1701	0.2476
H8	0.0672	0.1297	0.2171
H9	0.1218	0.1898	0.2701
O10	-0.2869	-0.2261	-0.0829
C11	-0.3586	-0.2582	-0.2094
C12	-0.2562	-0.1780	-0.1465
C13	-0.1092	-0.0146	0.0240
N14	-0.1568	-0.0353	0.0319
H15	0.0768	0.1604	0.2178
H16	0.1008	0.1838	0.2478
H17	0.1155	0.1947	0.2600
H18	0.2726	0.2958	0.3305

7

4.2 Quantum chemical calculations

4.2.1 Optimized structures

The optimized geometry of the probe was obtained using DFT/B3LYP method with 6-311++G (d, p)
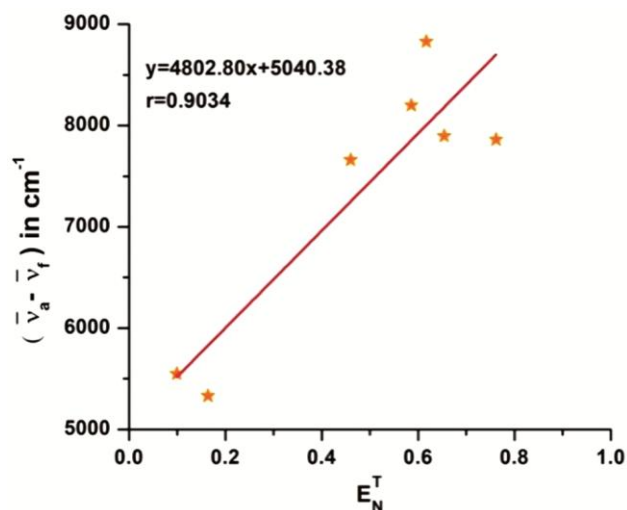
Fig.7 – The variation of Stoke's shift with E_T^N for QO

basis set via Gaussian 9W and are shown in Fig. 8. Theoretically calculated ground state dipole moments is found to be 2.814D for this QO compound given by Fig. 9 with direction of dipole moment. To obtain accurate values for the dipole moments in ground and excited energy states, the interaction of compound with the solvent molecules should be considered.

Unfortunately theoretical calculation assumes compounds in the gas phase and excludes solute-solvent interaction. This explains the observed discrepancy in theoretical and experimental dipole moments for this compound in our studies.

4.2.2 Frontier molecular orbital analysis

In computational Chemistry, energies and allocations of the frontier molecular orbital's are very imperative descriptors. Highest Occupied Molecular Orbital (HOMO) and Lowest Unoccupied Molecular
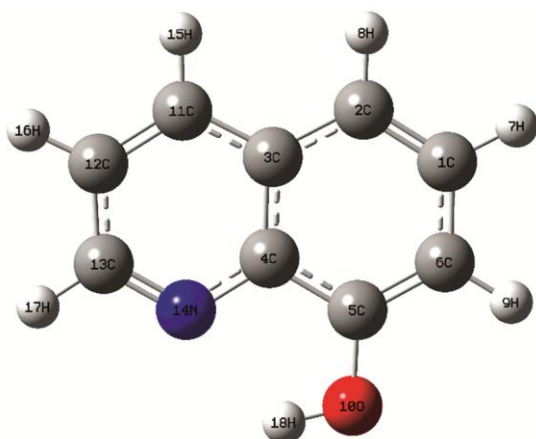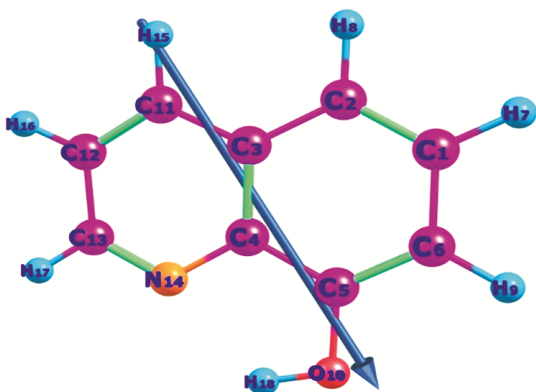
Fig. 8 – Optimized diagrams of QO

Fig.9 – Ground state optimized molecular geometries of QO. The arrow indicates the direction of the dipole moment.

Orbital (LUMO) help in demonstrating the chemical reactivity, active site/s, and kinetic stability of the molecule. HOMO represents electron donating ability of molecule (filled state) and LUMO represents the electron gaining ability (empty state). Energetic behavior of the dye under investigation is evaluated by Frontier Molecular Orbital calculations carried out by DFT/B3LYP with 6-311++G(d, p). Energy difference between these Frontier orbital's play an important role as an analytical parameter in resolving and understanding molecular transport properties. The 3D plots of HOMO-LUMO are presented in Fig. 10.

The large value of energy gap means a hard molecule and stability of the molecule can be related hardness and small energy gap means a soft molecule which indicates its more reactive nature. According to the Koopmans' theorem, ionization potential (IP) and electron affinity (EA) can be obtained as, EA= $-E_{LUMO}$ and IP= $-E_{HOMO}$. Electro negativity (χ) can be calculated as $\chi = (IP+EA)/2$ and chemical potential
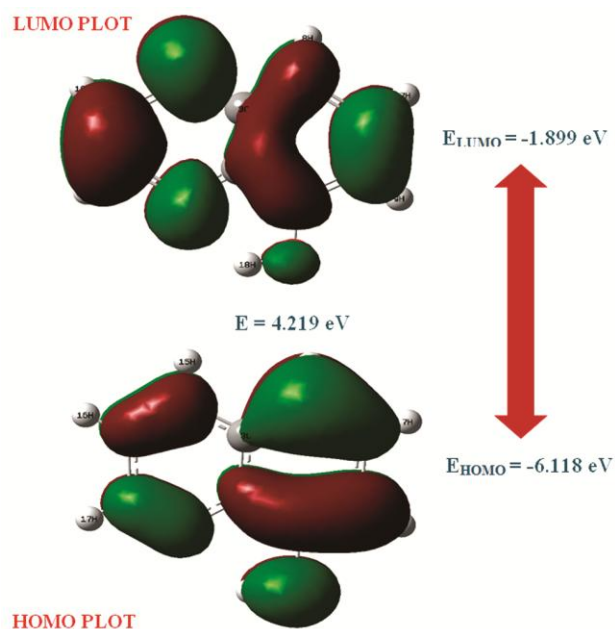

Fig.10 – HOMO-LUMO Structure of QO

(V) is a negative of electro negativity V= - (IP+EA)/2. The chemical hardness (η) which measures chemical stability is defined by $\eta = (IP-EA)/2$ and chemical softness (S) which measures chemical reactivity is inverse of chemical hardness defined as S= $1/\eta$. Energy is reduced between Frontier orbitals by extreme stream of electrons which is accounted as electrophilicity index defined as $\omega = \mu^2/2\eta$. The determined FMOs and related molecular properties values for the QO compound shown in Table 5. The calculated energy gap values for QO is 4.219 respectively. The calculated lower energy gap of the molecules confirms the delocalization of electron density present within the molecules, which enhances their molecular reactivity. The calculated higher ionization potential and the lower electron affinity values of QO compound reveal the possibility of electrophilic and nucleophilic attack.

4.2.3 *Molecular Electrostatic Potentials (MEP) and contour map analysis*

The electronic cloud surfaces are called Molecular Electrostatic Potentials (MEPs) are electronic cloud surfaces of the compound. The type of reactivity in a compound can be represented using this model. MEP shows the color indicated reactivity of the regions for being electrophilic or nucleophilic [34-55]. As we know that the neighboring molecules interact with each other through their potentials which could be approximated by the electrostatic potential [V(r)], by

ignoring the polarization and reorganization effects, given by Eq. (17):

$$V(r) = \sum \left[\frac{Z_R}{|R_A - r|} \right] - \int \left[\frac{\rho(r')dr'}{|r'-r|} \right] \qquad \dots (17)$$

where the summation ($\sum$) runs over all nuclei (A) of the molecule, Z_R is the charge of nucleus A located at R_A, $\rho(r')$ is the function of electron density of the molecule and r' is the dummy integration variable. The MEP of this compound is calculated and mapped on the optimized geometry. It is presented in Fig. 11 where characteristic increasing values of electrostatic potential on the surface are indicated by various colors in succession of red (represent electron rich or electrophilic reactivity)> orange > yellow> green > blue (represent electron deficient or nucleophilic reactivity). The color code of MEP diagram lies between -0.03957 a.u. (dark red) and 0.003957 a.u. (dark blue) for QO. Light blue region around Hydrogen atoms of Quinoline compound represent that they contain positive potential and that region is more electron deficient and hence nucleophilic in nature (electrophilic attack locale). Oxygen atoms of Quinoline groups are found to have deep red color indicating electron rich region and hence are analyzed to be more electrophilic in nature (nucleophilic attack locale).

Contour map of molecular electrostatic potential surface of this compound is shown in Fig. 12 which also confirms positive and negative regions of the molecule in accordance with total electron density surface. It is observed that there are closed contours for all 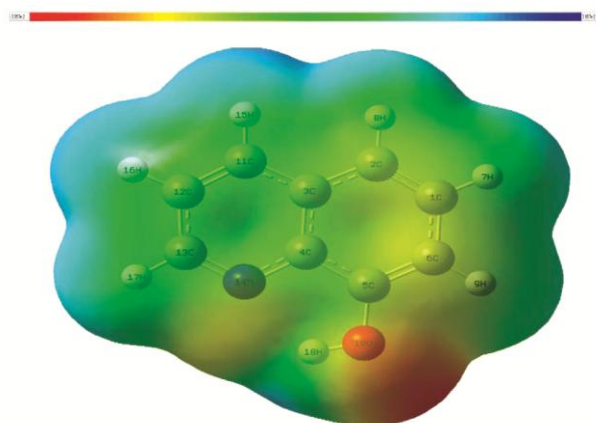oxygen atoms and inside each of the benzene rings. Both MEP and contour analysis represent the available sites for nucleophilic and electrophilic reaction.

4.2.4   *Mulliken atomic charges*

Atomic charges and charge transfer concept define molecular behavior and reactivity and hence analysis of atomic charges plays an important role in quantum chemistry. The atomic charges on the atoms are computed by Mulliken population study via B3LYP methods with 6-311++G (d, p) basis level. Mulliken charge distribution is shown in Fig. 13 and electronic charge values are listed in Table 6. Here there are total 18 atoms for QO.

4.2.5   *Fukui Function Analysis*

The Fukui function is among the most basic and commonly used reactivity indicators. The Fukui function is given as the change in the density function $\rho(r)$ of the molecule as a consequence of changing the number of electrons N in the molecule, under the constraint of a constant external potential. The Fukui function is defined as[56-63]:
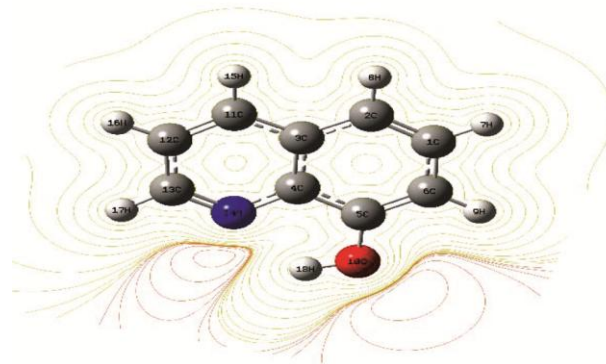
Fig. 12 – The contour map of molecular electrostatic potential surface for QO

Fig. 11 – The total electron density mapped with the MEP surface for QO
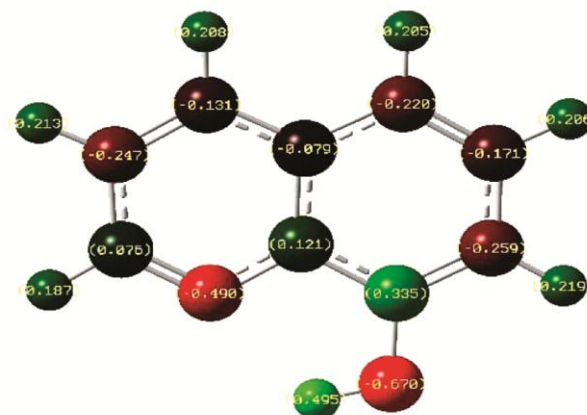
Fig. 13 – Mulliken charges for QO

$$F(r) = \frac{\partial \rho(r)}{\partial N} \qquad \dots (18)$$

where $\rho(r)$ is the electronic density, N is the number of electrons and r is the external potential exerted by the nuclease. Fukui functions are introduced, which are advocated as reactivity descriptors in order to identify the most reactive sites for electrophilic or nucleophilic reactions within a molecule. The Fukui function indicates the propensity of the electronic density to deform at a given position upon accepting or donating electrons. Also, it is possible to define the corresponding condensed or atomic Fukui functions on the jth atom site as,

$$f_j^- = q_j(N) - q_j(N-1) \qquad \dots (19)$$

$$f_j^+ = q_j(N+1) - q_j(N) \qquad \dots (20)$$

$$f_j^0 = \frac{1}{2}\left[q_j(N+1) - q_j(N-1)\right] \qquad \dots (21)$$

for an electrophilic f_j^- (r), nucleophilic f_j^+ (r)or free radical attack f_j^0 (r), on the reference molecule, respectively. In these equations, q_j is the atomic charge (evaluated from Mulliken population analysis, electrostatic derived charge, etc.) at the jth atomic site in the neutral (N), anionic (N + 1) or cationic (N - 1) chemical species. Here, it is important to mention that independently of the approximations used to calculate the Fukui function, all of them follow the exact Eq. (22):

$$\int f(r)\, dr = 1 \qquad \dots (22)$$

which is important in the use of the Fukui function as an intramolecular reactivity index. The values of the Fukui function are calculated from the NBO charges. The values of Fukui function analysis obtained by employing MEP and Mulliken charges[56-63].

The molecular reactivity plays a vital role in understanding bioactivity and for designing novel drug compound. In present investigation, the single point energy calculations are performed at the DFT/B3LYP 6-311++G (d, p) basis set for the anionic and cationic form of the QO molecules using the ground state with doublet multiplicity. The electron density based local reactivity descriptors such as Fukui functions (f_k^+, f_k^-, f_k^0), local softness (S_k^+, S_k^-, S_k^0) and local electrophilicity indices (ω_k^+, ω_k^-, ω_k^0) are calculated for all three molecules are listed in Table 7 using Mulliken population analysis shown in Table 6 to predict the possible electrophilic and nucleophilic reactive site of the molecule.

Table 7 depicts that for QO, the most nucleophilic reactive atoms are in the order of C2>O10 > H8 >H9. The atoms C2, H9 and H8 atoms present in the benzene ring, confirm that the benzene ring is the highly reactive site for a nucleophilic attack. The most electrophilic reactive atoms are identified to be in the order of N14 >C11>C3 >C13. All the atoms are present in the Quinoline ring, reveal that the Quinoline ring is the highly reactive site for an electrophilic attack. The C2, O10, N14 and C3 atoms are favorable sites for the radical attack.

Table 7 – Calculated Fukui functions, local softness and local eletrophilicity indices of QO.

Atoms	f_k^+	f_k^-	f_k^0	S_k^+	S_k^-	S_k^0	ω_k^+	ω_k^-	ω_k^0
C1	-0.0162	0.0227	0.0032	-0.0077	0.0107	0.0015	-0.0618	0.0863	0.0122
C2	0.1604	0.0815	0.1209	0.0760	0.0386	0.0573	0.6107	0.3103	0.4605
C3	0.0767	0.0971	0.0869	0.0364	0.0460	0.0412	0.2922	0.3699	0.3311
C4	-0.0855	-0.1213	-0.1034	-0.0405	-0.0575	-0.0490	-0.3256	-0.4620	-0.3938
C5	0.0325	-0.0267	0.0029	0.0154	-0.0126	0.0014	0.1236	-0.1016	0.0110
C6	0.0364	0.0227	0.0295	0.0172	0.0108	0.0140	0.1384	0.0865	0.1124
H7	0.0775	0.0691	0.0733	0.0367	0.0327	0.0347	0.2951	0.2631	0.2791
H8	0.0874	0.0625	0.0750	0.0414	0.0296	0.0355	0.3328	0.2380	0.2854
H9	0.0803	0.0680	0.0741	0.0380	0.0322	0.0351	0.3056	0.2589	0.2823
O10	0.1433	0.0607	0.1020	0.0679	0.0288	0.0483	0.5455	0.2312	0.3884
C11	0.0487	0.1004	0.0746	0.0231	0.0476	0.0354	0.1856	0.3825	0.2841
C12	0.0315	0.0782	0.0548	0.0149	0.0371	0.0260	0.1200	0.2977	0.2088
C13	0.0386	0.0945	0.0666	0.0183	0.0448	0.0316	0.1470	0.3600	0.2535
N14	0.0672	0.1215	0.0944	0.0319	0.0576	0.0447	0.2560	0.4627	0.3594
H15	0.0574	0.0836	0.0705	0.0272	0.0396	0.0334	0.2187	0.3184	0.2686
H16	0.0640	0.0830	0.0735	0.0303	0.0394	0.0348	0.2436	0.3162	0.2799
H17	0.0653	0.0792	0.0722	0.0309	0.0375	0.0342	0.2485	0.3016	0.2750
H18	0.0347	0.0232	0.0289	0.0164	0.0110	0.0137	0.1321	0.0882	0.1102

4.2.6 *Natural bonding orbital (NBO) analysis*

Investigation of intra- and intermolecular bonding analysis can be effectively carried out by NBO analysis tool and it provides a supportive modus operandi for examining charge transfer or hyper- conjugative interactions. NBO 5.0 software is used to perform rehybridization, intramolecular charge delocalization and electron density within molecule computed from Gaussian 9W software. Bonding and anti-bonding interactions owing to second-order perturbation are analyzed quantitatively by NBO approach that expresses perturbation energies E(2) by Eq. (23):

$$E(2) = \Delta E_{ij} = q_i \frac{F^2(i,j)}{\left(E_i - E_j\right)}$$

... (23)

where Ei and Ej are the diagonal elements, q_i is donor orbital occupancy and $F_{i,j}$ is NBO off-diagonal matrix element.

The most efficient interactions between the Lewis-type occupied NBO orbital (bonding) with non-Lewis unoccupied NBO orbital (anti-bonding) is calculated and listed in Table 8 for this QO compound. The nearby examination of the different donors and acceptors indicate that there are just two sorts of donors σ and π, and two kinds of acceptors σ* and π*. Between these donors and acceptors, observation of perturbation energy E_2 for different transitions shows the chances of the following transitions to be highly probable for QO, C1- C2 → C3-C4 (20.04 kj/mol, π→π*), C1-C2→C5-C6 (19.06 kj/mol, π→π*), C3-C4→ C5-C6 (19.86 kj/mol, π →π*) are the most

Table 8 – Second order perturbation theory analysis of Fock matrix in NBO basis of QO.

Donor(I)	Type of Band	Occupancy	Acceptor(J)	Type of Band	Occupancy	E2(Kj/mol)[a]	E(j)-E(i) (a.u)[b]	F(i, j) (a.u)[c]
C1-C2	σ	1.979	C2-C3	σ*	0.013	3.08	1.26	0.056
	σ	1.979	C3-H11	σ*	0.468	3.83	1.1	0.058
C1-C2	π	1.750	C3-C4	π*	0.040	20.04	0.29	0.07
	π	1.750	C5-C6	π*	0.021	19.06	0.28	0.065
C1-C6	σ	1.979	C5-O10	σ*	0.313	4.19	0.98	0.057
C1-H7	σ	1.979	C2-C3	σ*	0.013	3.51	1.1	0.055
	σ	1.979	C5-C6	σ*	0.022	3.19	1.08	0.052
C2-C3	σ	1.979	C3-C4	σ*	0.014	3.91	1.28	0.063
	σ	1.979	C4-N14	σ*	0.468	3.58	1.07	0.055
C2-H8	σ	1.979	C1-C6	σ*	0.278	3.39	1.09	0.054
	σ	1.979	C3-C4	σ*	0.014	4.3	1.1	0.062
C3-C4	σ	1.979	C2-C3	σ*	0.013	3.91	1.28	0.063
	σ	1.979	C4-C5	σ*	0.023	3.78	1.27	0.062
	σ	1.979	C5-O10	σ*	0.313	3.52	0.99	0.053
C3-C4	π	1.750	C1-C2	π*	0.013	17.63	0.28	0.065
	π	1.750	C5-C6	π*	0.021	19.86	0.28	0.068
	π	1.750	C11-C12	π*	0.239	9.51	0.29	0.05
	π	1.750	C13-N14	π*	0.319	9.48	0.28	0.049
C3-C11	σ	1.979	C12-H16	σ*	0.013	3.13	1.08	0.052
C4-C5	σ	1.979	C3-C4	σ*	0.014	4.08	1.29	0.065
	σ	1.979	C3-C11	σ*	0.468	3.1	1.12	0.053
	σ	1.979	C5-C6	σ*	0.022	3.05	1.26	0.055
C5-C6	σ	1.979	C4-C5	σ*	0.023	3.4	1.27	0.059
	σ	1.979	C4-N14	σ*	0.468	4.12	1.07	0.059
C5-C6	π	1.750	C1-C2	π*	0.013	20.1	0.29	0.068
	π	1.750	C3-C4	π*	0.040	18.7	0.29	0.068
C6-H9	σ	1.979	C1-C2	σ*	0.000	3.59	1.09	0.056
	σ	1.979	C4-C5	σ*	0.023	3.77	1.09	0.057
O10-H18	σ	1.979	C5-C6	σ*	0.021	3.6	0.74	0.05
C11-C12	π	1.750	C3-C4	π*	0.040	9.56	0.31	0.052
	π	1.750	C13-C14	π*	0.319	12.92	0.3	0.055
C11-H15	σ	1.979	C12-C13	σ*	0.026	4.69	0.92	0.059
C12-C13	σ	1.979	C11-H15	σ*	0.015	3.52	1.08	0.055
C12-H16	σ	1.979	C3-C11	σ*	0.468	4.9	0.94	0.061
C13-N14	π	1.750	C3-C4	π*	0.040	10.58	0.34	0.058
	π	1.750	C11-C12	π*	0.239	7.31	0.34	0.045
C13-H17	σ	1.979	C4-N14	σ*	0.468	6.35	0.91	0.068

[a]E2 means energy of hyper conjugative interactions. [b]Energy difference between donor and acceptor i. and j. NBO orbitals.[c] F(i, j) is the Fock matrix element between i .and j. NBO orbitals

Table 9 – Calculated and observed UV-vis spectral parameters and its assignments of QO in 1,4-dioxane solution.

Theoretical				Experimental		
Contribution of orbitals	λ (nm)	E(eV)	f	λ (nm)	E(eV)	Assignments
H→L(69%)	337	3.67	0.053	331	3.76	n→π*
H→L+1(55%) H-1→L(43%)	287	4.31	0.005			π→π*

where, H-HOMO, L-LUMO, λ-wavelength, E-excitation energies and f-oscillator strength

probable transitions. These possible changes reveal that transitions which happen here are just inside the Phenyl ring, focused on the carbon atoms through which substitutions are associated with the ring. These transitions represent greater contributions from π-electrons having strong Intramolecular hyper conjugative interaction. The $\pi \rightarrow \pi^*$ transitions in this molecule account for the high polarization and which is further responsible for the NLO activity of the molecule.

4.2.7 *Ultraviolet-visible spectral analysis*

The UV-vis spectral analysis is carried out in order to understand the nature of the electronic transitions of QO compound. Table 9 depicts the calculated and experimental electronic transition properties such as absorption wavelength (λ), excitation energy (E), oscillator strength (f), the contribution of orbitals and assignments of electronic transitions. The observed and simulated UV-vis spectra are shown in Fig. 14. The calculated electronic transition is obtained at 337 nm and the corresponding electronic transition was observed at 331 nm, which is assigned to the n→π* transitions of the compound. This n→π* transitions, which arises due to the electronic transitions from a lone pair of electrons present in the electronegative atoms to π electrons in the compound[64]. The calculated electronic transition peak is obtained at 287 nm, which are assigned to the $\pi \rightarrow \pi^*$ electronic transition of the compound. The $\pi \rightarrow \pi^*$ transitions indicate the presence of hyper-conjugation interactions in the Phenyl ring. From UV spectrum, the theoretical calculations predict one band located at 287 nm with an oscillator strength 0.005. The highest absorbed band is observed at 337 nm with an oscillator strength 0.053 which transition is due to the contribution of HOMO/LUMO with 69%.

5 Conclusions

Following inferences are drawn from the above discussion, we have studied the spectroscopic behavior and quantum chemical computations for this compound QO.
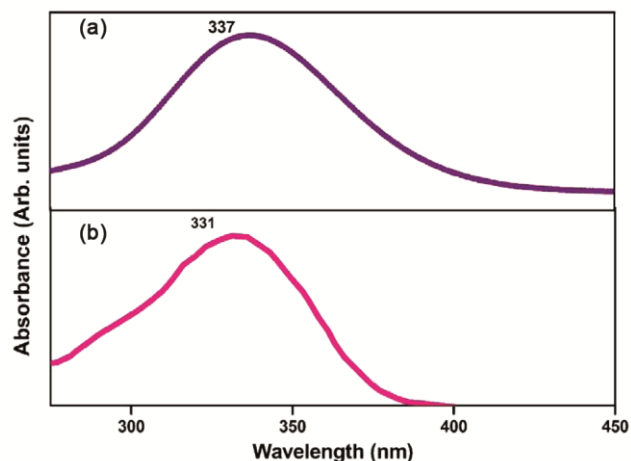

Fig. 14 – The UV-vis spectra of QO (a) theoretical and (b) experimental

(i) It is found that excited state dipole moment (μ_e) is greater than ground state dipole moment (μ_g) for this compound. The ground state and excited state dipole moment results are correlated with experimental and theoretical values in this study. The discrepancies observed in the calculated values of the ground and excited state dipole moments from equations may be due to approximations made in all methods to estimate ground state and excited singlet state dipole moments for this compound.

(ii) A bathochromic shift in Stokes shift is observed with an increase in the solvent polarity which confirms π→π* transition in this molecule together with ICT character.

(iii) The calculated lower value of HOMO-LUMO energy gap of this compound shows the high molecular reactivity of the studies compounds which are explained by the analysis of molecular electrostatic potentials, contour studies and Fukui function analysis. The intramolecular interactions of the molecule are also confirmed through NBO analysis and possible electrophilic and nucleophilic reactive sites are predicted. The calculated Fukui functions infers the local softness and

local electrophilicity indices of used all solute molecules. UV-Visible spectrum is simulated theoretically and experimentally validated by the observed absorption peak.

References

1   Lackowicz J R, *Principle of Fluorescence Spectroscopy*, Plenum Press, New York (1983).
2   Rohtagi–Mukherjee K K, *Fundamentals of Photochemistry*, Wiley Eastern Ltd, (1992).
3   Musa M A , Wood J S C & Khan M O F , *Curr Med Chem*, 15 (2008) 2664.
4   Lei L, Xue Y B, Liu Z, Peng S S, He Y, Zhang Y, Fang R, Wang J P, Luo Z W, Yao G M, Zhang J W, Zhang G, Song H P & Zhang Y H, *Sci Rep*, 5 (2015) 13544.
5   Collin G & Höke H, Quinoline and Isoquinoline, Ullmann's Encyclopedia of Industrial Chemistry, Weinheim: Wiley-VCH, (2005)doi:10.1002/14356007.a22_465.
6   Kawski A, Kuklinski B & Bojarski P, *Chem Phys Lett*, 448 (2007) 208.
7   Muddapur G V, Patil N R , Patil S S , Melavanki R M & Kusanur R A , *J Fluoresc*, 24 (2014) 1651.
8   Patil S S, Muddapur G V, Patil N R, Melavanki R M & Kusanur R A, *Spectrochim Part A Mol Biomol Spectros*, 138 (2015) 85.
9   Lippert E, *Z Elektrochem*, 61 (1957) 962.
10 Bakshiev N G, *Opt Spectrosk*, 16 (1964) 821.
11 Bilot L & Kawski A, *Z Naturforsch*, 18 (1963) 10.
12 Chamma A, Viallet P & Acad C R, *Sci Paris Ser C*, 270 (1970) 1901.
13 Katritzky A R, Fara D C, Yang H, Tamm K, Tamm T & Karelson M, *Chem Rev*, 104 (2004) 175.
14 Reichardt C, Solvents and Solvent Effects in Organic Chemistry, 2ⁿᵈ Edn, VCH, 1988.
15 Muddapur G V, Koppal V V, Patil N R & Melavanki R M, *AIP Conf Proc*, 1728 (2016) 020373.
16 Muddapur G V, Melavanki R M, Patil P G, Nagaraja D & Patil N R, *J Mol Liq*, 224 (2016) 201.
17 Koppal V V, Muddapur G V, Patil N R & Melavanki R M, *AIP Conf Proc*, 1728 (2016) 020411.
18 Desai V R, Sidarai A H, Hunagund S M, Basanagouda M, Melavanki R M, Fattepur R H & Kadadevarmath J S, *J Mol Liq*, 223 (2016) 141.
19 Koppal V V, Muddapur G V, Patil N R & Melavanki R M, *AIP Conf Proc*, 1728 (2016) 020411.
20 Sharma K, Melavanki R, Patil S S, Kusanur R, Patil N R & Shelar V M, *J Mol Struct*, 1181 (2019) 474.
21 Kirilova E, Yanichev A, Puckins A, Fleisher M & Belyakov S, *Luminescence*, (2018)1. wileyonlinelibrary.com/journal/bio
22 Geethanjali H S, Nagaraja D & Melavanki R M , *J Fluoresc*, 25 (2015) 745.
23 Patil N R, Melavanki R M, Kapatkar S B, Ayachit N H & J Saravanan, *J Flurosec*, 21 (2011) 1213.
24 Melavanki R M, Patil H D, Umapathy S & Kadadevarmath J S, *J Fluoresc*, 22 (2012) 137.
25 Kadadevarmath J S, Malimath G H, Patil N R, Geethanjali H S & Melavanki R M, *Can J Phys*, 91 (2013) 1107.
26 Patil P G, Koppal V V, Melavanki R M & Patil N R, *Mater Today Proc*, 5 (2018) 2781.

27 Bhavya P, Melavanki R, Manjunatha M N, Koppal V, Patil N R & Muttannavar V T, *AIP Conf Proc*, (1953) 080022.
28 Koppal V V, Patil P G, Melavanki R M & Patil N R, *Mater Today Proc*, 5 (2018) 2759.
29 Bhavya P, Melavanki R, Sharma K, Kusanur R, Patil N R & Thipperudrappa J, *Chem Data Collect*, 19 (2019) 100182.
30 Raghavendra U P, Basanagouda M, Melavanki R M, Fattepur R H, Thipperudrappa J, *J Mol Liq*, 202 (2015) 9.
31 Sıdır Y G & Sıdır I, *Spectrochim Acta Part A*, 102 (2013) 286.
32 Zakerhamidi M S, Ahmadi-Kandjani S, Moghadam M, Ortyl E & Kucharski S, *J Mol Struct*, 996 (2011) 95.
33 Gilani G, Hosseini S E, Moghadam M & Alizadeh E, *Spectrochim Acta Part A*, 89 (2012) 231.
34 Atilgan A , Yurdakul Ş, Erdogdu Y & Güllüoğlu M T, *J Mol Struct*, 1161 (2018) 55.
35 Gaddam R & Reddy B V, *J Mol Struct*, 1160 (2018) 271.
36 Khajehzadeh M & Sad N, *J Mol Liq*, 249 (2018) 281.
37 Wazzan N A, Al-Qurashi Ohoud S & Faidallah H M , *J Mol Liq*, 223 (2016) 29.
38 Srivastava R, Al-Omary F A M, El-Emam A A, Pathak S K , Karabacak M, Narayan V, Chand S, Prasad O & Sinha L, *J Mol Struct*,1137 (2017) 725.
39 Al-Ahmary K M, Mekheimer R A, Al-Enezi M S, Hamada N M M & Habeeb M M, *J Mol Liq*, 249 (2018) 501.
40 Mohbiya D R & Sekar N, *Chem Select*, 3 (2018) 1635.
41 Tanak H, Agar A & Metinyavuz, *Int J Quant Chem*, 111 (2011) 2123.
42 Premkumar S, Jawahar A, Mathavan T, Dhas M K & Benial A M F, *Spectrochim Acta Part A*, 138 (2015) 252.
43 Premkumar S, Jawahar A, Mathavan T, Dhas M K, Sathe V G, Franklin B A M, *Spectrochim Acta Part A*,129 (2014), 74.
44 Premkumar S, RekhaBeulah T N, Rajkumar J M, Asath R M, Jawahar A, Mathavan T & Benial A M F, *Braz J Phys*, 45 (2015) 621.
45 Premkumar S, Rekha T N R, Asath M, Mathavan T & Benial A M F, *Euro J Pharma Sci*, 82 (2016) 115.
46 Premkumar S, Rekha T N, Asath R M, Jawahar A, Mathavan T & Benial A M F, *J Mol Struct*, 1107 (2016) 254.
47 Muttannavar V T, Melavanki R, Bhavya P, Kusanur R, Patil N R & Naik L R, *Int J Life Sci Pharma Res*, 8 (2018) 24.
48 Gaussian09 RA. 1, Frisch M J, Trucks G W, Schlegel H B, Scuseria G E, Robb M A, Cheeseman J R, Scalmani G, Barone V, Mennucci B, Petersson G A, Gaussian Inc, Wallingford CT, 2009.
49 Frisch A, Nielsen A B, Holder A J, Gaussview user manual, Gaussian Inc, Pittsburgh, PA, (2000) 556.
50 Dengton R, Keith T, Millam J, Eppinnett K, Hovell WL & Gilliland R, Gauss View, Version 309, Semichem. Inc, Shawnee Mission, KS 2003.
51 Glendening E D, Reed A E, Carpenter J E, Weinhold F, NBO Version 3.1, TCI University of Wisconsin, Madison, (1998) 65.
52 Wohlfarth C, Static dielectric constants of pure liquids and binary liquid mixtures: supplement to IV/6. Springer Science & Business Media; 2008 Apr 25.
53 Suppan, *J Chem Soc A*, 3125 (1968); Suppan P & Tsiamis C, *Spectrochim Acta Part A*, 36 (1980) 971.
54 Reichardt C, *Chem Rev*, 94 (1994) 2319.
55 Ravi M, Soujnya T, Samanta A & Radhakrishnan T P, *J Chem Soc Faraday Trans*, 91 (1995) 2739.

56 Premkumar S, Rekha T N, Asath R M, Mathavan T & Benial A M Frank, *Eur J Pharm Sci*, 82 (2016) 115.

57 Premkumar S, Rekha T N, Asath R M, Jawahar A, Mathavan T & Benial A M F, *J Mol Struct*, 1107 (2016) 254.

58 Demircioğlu Z, Kaştaş Ç A & Büyükgüngör O, *Spectrochim Acta Part A: Mol Biomol Spectrosc*, 139 (2015) 539.

59 Avdović E H, Milenković D, Marković J M D, Đorović J, Vuković N, Vukić M D, Jevtić V V, Trifunović S R, Potočňák I, Marković Z, *Spectrochimica Acta Part A; Mol Biomol Spectrosc*, 195 (2018) 31.

60 Parr R G & Yang W, *J Am Chem Soc*, 106 (1984) 4049.

61 Fukui K, Theory of orientation and stereo selection, Springer-Verlag, Berlin (1975).

62 Shu-BIN L I U, Conceptual Density Functional Theory and Some Recent Developments, *Acta Phys Chim Sin*, 25 (2009) 590.

63 http://www.molinspiration.com/cgi-bin/properties

64 Rao Y B S, Prasad M V S, Udaya N S, Veeraiah V, *J Mol Struct*, 1108 (2016) 567.